Attractive forces in sterically stabilized colloidal suspensions: From the effective potential to the phase diagram

J. G. Malherbe,* C. Regnaut, and S. Amokrane
Groupe de Physique des Milieux Denses, Faculté des Sciences et de Technologie, Université Paris XII–Val de Marne, 61 Avenue du Général de Gaulle, 94010 Créteil Cedex, France
(Received 26 June 2002; published 18 December 2002)

The potential of mean force for macroparticles at infinite dilution is computed for several models of solvent-solvent and solvent-macroparticle interactions by using the reference hypernetted chain (RHNC) integral equations with Rosenfeld's density functional theory bridge functions. The phase diagram of the associated effective fluid is obtained from the RHNC free energy for the fluid branch and the perturbation theory for the solid one. The computation of the effective potential and of the fluid branch is tested by comparison with Monte Carlo simulation. The important modifications with respect to the pure hard spheres that were previously reported are confirmed. The possibility of inverting the relative stability of the fluid-fluid and the fluid-solid transitions by appropriate combination of the interaction parameters is shown. The importance of a fine description of the interactions is illustrated in the example of the role of the range of the solvent-solvent interaction potential.

DOI: 10.1103/PhysRevE.66.061404 PACS number(s): 64.70.−p, 82.70.Dd, 61.20.Gy

I. INTRODUCTION

Understanding the phase behavior of colloidal suspensions and predicting it from a microscopic approach is still a great challenge in the physics of liquids. Indeed, these systems exhibit particular features that distinguish them from simple fluids or ordinary mixtures and make their theoretical study more difficult [1,2]. To take the example of sterically stabilized colloids suspended in an ordinary solvent—the actual physical systems that motivated this study—their first unusual characteristic is the big difference in size between solvent and solute particles (hereafter, small and large particles will be referred to as components 1 and 2). This purely geometrical asymmetry being a generic property of colloids, its consequences have been investigated in numerous theoretical studies based on the asymmetric binary hard sphere (HS) mixture model. The sole parameter of this model is the diameter ratio $R=D_2/D_1 \gg 1$ and the relevant thermodynamic variables are the packing fractions $\eta_i = (\pi/6)\rho_i D_i^3$ (ρ_i is the number density of component i). However, the behavior of this model for $R \gg 1$ came to be understood on the whole only recently (see, for example, Refs. [3,4] and references therein), because of several technical difficulties. On one hand, the accuracy of standard methods based on the Ornstein Zernike equations (OZE) is uncertain since their sensitivity to approximate closures becomes more critical as R increases [5]. This prompted the use of an alternative route based on the density functional theory (DFT) (see Refs. [6,7]). On the other hand, computer simulations that might validate the theoretical methods are equally problematic: first because the number N_1 of small particles required to achieve comparable packing fractions rapidly becomes prohibitive (the ratio N_1/N_2 increases as R^3), second because the solute particles are artificially ''frozen'' by the presence of the solvent, with a resulting poor statistics. Many efforts have been made to tackle these problems. From the point of view of simulations, specialized algorithms have been developed [8–10] that made it possible to go beyond the early results of Jackson *et al.* [11]. On the other hand, various improvements of the integral equations [12–15] (IE) and DFT (see, for example, Refs. [6,7]) approaches have been proposed. In this way, Biben and Hansen [16] detected a phase instability in sufficiently asymmetric HS mixture with the Ballone *et al.* [13] and the Rogers and Young [12] IE, a result substantiated by new simulation data obtained by the configuration bias Monte Carlo method [8]. Even though the underlying mechanism (the depletion effect) was known for quite a long time (see the work of Asakura and Oosawa [17], and that of Vrij [18]), this was a surprising result, since it contradicted the conclusion drawn by Lebowitz and Rowlinson [19] from the Percus- Yevick (PY) closure [20] which predicts a homogeneous HS mixture at all packing fractions and size ratios. This phase transition driven by purely entropic effects became thus a source of great interest that finally yielded a well established phase diagram, first computed by Dijkstra *et al.* [3] (see references therein for the related work). The main conclusion is that a sufficiently asymmetric hard sphere mixture shows both a fluid-solid (F-S) and a fluid-fluid (F-F) transition but the latter is always metastable.

These results relative to the depletion effect are of course of fundamental value but the remaining question is the relevance of the underlying model to real colloids. Some colloids might indeed behave as hard spheres but the associated universal phase diagram is not the generic one for a quite large number of colloidal suspensions. Indeed, if all actual mixtures were hard-sphere-like, it would be impossible to observe for example a dense fluid of solute particles suspended in a liquid solvent ($\eta_1 \sim 0.4$). This is obviously different from the behavior of many real colloids that often show stable fluid phases that are rich in solute particles [1,2].

*Author to whom correspondence should be addressed. email address: malherbe@univ-paris12.fr

Also, temperature often plays a major role (a striking example is the lower consolute point observed in some reverse micellar systems [21]) in contrast with the case of pure hard spheres for which it is not a relevant thermodynamic variable. Furthermore, experiments on real colloids, such as coated silica particles in organic solvents, show that the effective interaction between the solutes may be turned from attractive to repulsive by changing the nature of the solvent (see, for e.g., Ref. [22]), even when the solvent particles are of similar size. The composition of the surface layer of reverse micelles is also known to have a strong impact on their phase behavior (see, e.g., Ref. [23]).

All these features being foreign to the HS model, one needs to go further in the modeling by taking into account specific interactions between the components. The early attempts to introduce attractive forces based on Baxter's sticky hard sphere model [24] (see, e.g., Refs. [25–30] and references therein) gave useful indications, in particular on the crucial role played by heteroadhesions (solvation forces). This model, however, ignores the range of the interaction potentials u_{ij} between components and more realistic models such as the Yukawa or the Lennard-Jones (LJ) potentials were considered, first at the level of the potential of mean force at infinite dilution Φ^{eff} (for earlier work, see, for example, [31,32]). Attractive forces were more recently considered in Refs. [33,34] and similar studies of charged systems can be found for example in Refs. [35–37]. These studies have shown that this improved description of the interactions u_{ij} can have a strong impact on the potential of mean force. The same observation can be made from the nonadditive HS model [38–40].

These modifications are of course expected to exert an equally strong influence on the phase behavior. However, with the exceptions of a previous work from our group [41] and that of Louis *et al.* [38] on the phase diagram of the nonadditive HS mixtures, all other investigations of the role of attractive forces were limited to the changes they induce on the potential of mean force or on structural quantities (see also Ref. [42] for a discussion of nonadditive HS). The main goal of the present work is thus to discuss in more detail the influence of attractive forces on the phase diagram. In particular, we will analyze the prediction [41] that the relative position of the F-F and F-S coexistence lines can even be inverted when compared to hard spheres. On the other hand, the theoretical determinations of Φ^{eff} always involve approximations. It is thus important to test them by simulation in order to gain confidence in their predictions on the role of the attractions. From the simulation point of view, the situation is even more problematic than with pure HS systems. Indeed, in addition to the difficulties mentioned above in the pure HS case, one needs to monitor the difference in energy between successive configurations that might involve several thousand small particles. Besides our previous results [43] (size ratio $R=5$) and those presented in this paper ($R=10$), we are only aware of the simulation data of Shinto *et al.* [44] ($R=10$) and the recent work of Louis *et al.* [45] ($R=5$). This progressive accumulation of simulation data will help validate the various theoretical routes to obtain Φ^{eff}. This was already started in our recent work [46] in which different methods for computing Φ^{eff} were compared. From this study completed by the recent data presented here, it appears that the RHNC closure of the OZE with bridge functions B_{ij} computed from Rosenfeld's Fundamental Measure Functional (FMF) is the most reliable method for obtaining the effective potential (this method will be referred to as the RHNC/FMF). A similar discussion has been made in Ref. [45] for Φ^{eff} computed with the DFT, but the simulation data were for lower size ratio and solvent density than those we used to test the RHNC/FMF method.

In order to compute the phase diagram, the mixture was treated in these studies at the effective one-component fluid level with assumed pairwise additive interactions. In this approach (MacMillan-Mayer theory [47]), the focus is on the fluid of solute particles, the influence of the solvent being incorporated into the effective pair interaction Φ^{eff} which is computed given some model for the interaction potentials u_{ij} between components. Φ^{eff} is used in a second step to obtain the phase diagram of the effective fluid by methods appropriate to one-component fluids. Among these, the reference hypernetted chain (RHNC) [48] integral equation used in this work as in our previous ones [41,49] is known to be one of the most accurate. For the solid phase, we used the perturbation theory [50] which is accurate enough for interactions having the characteristics of Φ^{eff} (see Ref. [49] for a recent discussion of this point). Besides being computationally more convenient than a direct study of the true mixture, this effective fluid approach is the only one which can be tested at each step by simulation with present algorithms. Since—as discussed below—the two steps for computing the phase diagram do indeed test favorably by simulation, we now have a robust theoretical scheme for studying complex models of colloidal suspensions. It permits the analysis of the connection between the phase diagram and the microscopic parameters of the system. In this framework, we will present an example of a combination of interactions u_{ij} that leads to a stable dense fluid phase of solute particles in a dense solvent. This possibility remedies the most undesirable feature of the HS phase diagram when dealing with suspensions in which significant attractive forces are expected.

To this end, this paper is organized as follows. We first recall the theoretical background for computing the phase diagram for a given microscopic model. Then we confirm by simulation that the RHNC integral equation is accurate enough for studying the F-F transition. In the following part, we study the RHNC phase diagram of two different models and the relation between the effective interaction and the phase behavior. In particular, we try to clarify the role of the range of the solvent-solvent attraction by studying the effective potential by simulation and the integral equation method.

II. THE EFFECTIVE FLUID APPROACH

As stressed in the Introduction, the study will be conducted here at the effective one-component fluid level [47] because of the lack of validated theoretical methods for a direct treatment of the mixture. The binary mixture is reduced to an effective one-component fluid of solute particles

and the presence of the solvent is replaced by an effective pair interaction computed at infinite dilution of the solute. This reduction is detailed for example in Refs. [3,51]. Once the effective pair interaction Φ^{eff} is known, the phase boundaries of the effective fluid are obtained from the Helmholtz free energy by the common tangent construction.

A. The pair potential approximation

The potential of mean force $\Phi(R^{N_2};\mu_1)$ for N_2 solute particles immersed in a pure solvent at fixed chemical potential μ_1 is defined from the solute distribution function $\rho^{N_2}(R^{N_2};\mu_1;V;T)$ in the semigrand ensemble [47]. Its formal expression involves a sum over all numbers N_1 of small particles of the integral over their coordinates r^{N_1} of the Boltzmann factor $\exp[-\beta\Sigma_{i<j}u_{11}(r_{ij})+\Sigma_{i,J}u_{12}(r_i,R_J)]$, where u_{11} and u_{12} are the solvent-solvent and the solute-solvent interaction potentials and $\beta=1/k_BT$. This expression is, however, so intractable that the pairwise additivity assumption is usually invoked to permit the reduction of the binary mixture to an effective one-component fluid. In this approximation, one considers this N_2-body potential as the sum of two-body effective interactions

$$\Phi(R^{N_2};\mu_1)\sim\sum_{I<J}^{N_2}\Phi^{eff}(R_I,R_J;\mu_1). \tag{1}$$

The exact $\Phi(R^{N_2};\mu_1)$ is nonadditive because the solvent distribution about a given set of solute particles cannot be expressed solely in terms of its distribution $\rho^1(r;R_I,R_J)$ about pairs (I,J). Even if arguments might be invoked to justify this, analytical studies of correlations at the three particles level (see, e.g., Ref. [52] for the Lennard-Jones fluid) show that the presence of a third particle in the vicinity of a pair changes the distribution of the remaining ones about the pair. In a mixture, this effect is expected to increase with η_1, as confirmed by our previous simulation of the HS model [53]. Many-body effects were indeed detected even at high size ratio ($R=20$). These were expected to slightly shift the coexistence lines towards higher values of the solvent packing fraction in the reservoir. For more general models, however, this point needs to be clarified and remains the only uncontrolled approximation of this treatment.

Within this assumption of pairwise additivity of $\Phi(R^{N_2};\mu_1)$, the effective fluid of solute particles interacting via Φ^{eff} is then studied by standard methods for one-component fluids.

B. Phase boundaries of the effective fluid

In the semigrand ensemble, the solvent is characterized by its chemical potential or at fixed temperature, by the solvent density in the reservoir (it will be convenient to work with the reduced density $\rho^*\equiv\rho_1(D_1^{HS})^3$, where D_1^{HS} is defined below). In the construction of the fluid and solid branches of the iso-ρ^* free energies for the solute particles, it is assumed that the solvent remains in a single phase (this means that we are not considering the full phase diagram of the binary mixture). Therefore, when we explore different values of ρ^* a given choice of the solvent interaction parameters might actually correspond either to a supercritical solvent or to a temperature outside the coexistence domain in the $(T-\rho^*)$ plane.

1. The fluid branch

The fluid branch of the effective fluid is obtained by computing the RHNC free energy. The well-known RHNC integral equation is detailed in Ref. [48] to which we refer for explicit expressions of F_{RHNC}. It supplements the Ornstein-Zernike equation [50] for the total and direct correlation functions $h(r)=g(r)-1$ and $c(r)$:

$$h(r)-c(r)=\rho\int d\mathbf{r}'h(r')c(|\mathbf{r}-\mathbf{r}'|) \tag{2}$$

by the closure

$$g(r)=\exp[-\phi(r)/k_BT+h(r)-c(r)-b_0(r)], \tag{3}$$

where the interaction potential $\phi(r)$ corresponds here to Φ^{eff} defined above. $b_0(r)$ is the bridge function of a reference system, here a system of hard spheres, whose diameter σ_{HS} is determined by the optimization condition [54]

$$\int d\mathbf{r}[g(r)-g_0(r)]\frac{\partial b_0(r)}{\partial\sigma_{HS}}=0. \tag{4}$$

The RHNC has been applied to a variety of state independent interactions and has been shown to be very accurate when compared with simulation [see, for example, Refs. [5,55,56] and references therein]. In this work, we used the parametrization of $b_0(r)$ of Malijesvsky and Labik [57] and used the algorithm of Labik *et al.* [58] for solving Eqs. (2)–(4). This closure will be tested in our particular case of an effective potential exhibiting both long range tails as the LJ model and complex structures as depletion potentials. For the range of thermodynamic variables and interaction parameters considered here, it is almost as accurate as that computed using Rosenfeld's DFT [59]. But since it allows a much faster numerical solution of Eqs. (2)–(4) it was preferred in the computation of the iso-ρ^* free energies. In the (ρ^*,ρ_2) domain where numerical convergence is not possible, we followed the strategy detailed in Ref. [41]. The behavior of Φ^{eff} being less extreme when attractive forces are considered, the extent of the nonconvergence domain is in most cases much smaller than with pure HS.

2. The solid branch

To determine the F-S coexistence line the solid branch of the free energy F_S was obtained from a variational perturbation theory (VPT):

$$F_S(\rho_2)=F_{HS}(\rho_2)+\langle\Phi_{eff}-\Phi_{HS}\rangle_{HS}. \tag{5}$$

The technical details of our calculations of F_S were identical to those in the study of the Yukawa potential by Hasegawa [60] and in Refs. [41,49]. The accuracy of this scheme has been discussed in detail in Ref. [49] where it was shown that

at the densities ρ_2 of the solid state, the perturbation treatment of a short range interaction as Φ^{eff} is sufficiently accurate.

C. Potential of mean force at infinite dilution

1. General expression of Φ^{eff}

The potential of mean force $\Phi^{eff}(r;\mu_1)$ between a pair of solute particles separated by a distance r immersed in a pure solvent at chemical potential μ_1 can be obtained from the distribution function of solute particles at infinite dilution

$$g_{22}(r;\rho_2\to 0,\mu_1)=\exp[-\beta(u_{22}(r)+\Phi^{eff}(r;\mu_1)], \quad (6)$$

u_{22} being the direct interaction between the pair. In practice, at fixed T, the solvent bulk density ρ^* is used as the independent variable as mentioned above.

2. The integral equations route

In the IE route to Φ^{eff}, the solute pair distribution function (pdf) g_{22} is computed by taking the limit $\rho_2\to 0$ of the OZE [50]:

$$\gamma_{ij}(r)=\sum_k \rho_k \int d\mathbf{r}' c_{ik}(r')h_{kj}(|\mathbf{r}-\mathbf{r}'|), \quad (7)$$

where $\gamma_{ij}=h_{ij}-c_{ij}$ is the series function (with h_{ij} and c_{ij} the total and direct correlation functions). For a binary mixture, Eq. (7) must be supplemented by three closures,

$$g_{ij}=\exp\{-\beta u_{ij}+\gamma_{ij}-b_{ij}\}, \quad (8)$$

where b_{ij} is the bridge function. In the limit $\rho_2\to 0$, the equation for the solvent is uncoupled from the remaining ones:

$$\gamma_{11}(r)=\rho_1 \int d\mathbf{r}' h_{11}(r')c_{11}(|\mathbf{r}-\mathbf{r}'|). \quad (9)$$

The resulting c_{11} is fed into the equation

$$\gamma_{12}(r)=\rho_1 \int d\mathbf{r}' h_{12}(r')c_{11}(|\mathbf{r}-\mathbf{r}'|) \quad (10)$$

to obtain h_{12} and c_{12}, the final input in the equation giving γ_{22}:

$$\gamma_{22}(r)=\rho_1 \int d\mathbf{r}' h_{12}(r')c_{12}(|\mathbf{r}-\mathbf{r}'|). \quad (11)$$

In this paper we will consider two different closures. The HNC closure, in which one takes $b_{ij}=0$ gives

$$\beta\Phi^{eff}_{HNC}(r;\rho_1)=-\gamma_{22}(r). \quad (12)$$

This closure is easy to implement but is not accurate enough, especially for non-hard-core interactions [46]. It was employed here only for the comparison with the results obtained from the more sophisticated and very accurate RHNC/FMF closure using the b_{ij} obtained from Rosenfeld's DFT. In the RHNC (see, e.g., Refs. [14] and [31] for macroparticles in a solvent) one has

$$\beta\Phi^{eff}_{RHNC}(r;\rho_1)=-\gamma_{22}(r)+b_{22}(r), \quad (13)$$

where $b_{22}(r)$ is the bridge function for solutes at infinite dilution. We note here that the evaluation from the FMF of the $b_{ij}(r)$ in the test particle limit, $b_{ti}[\{\rho_i(\mathbf{r});r\}]=\beta(\mu^{HS}_{i,ex}[\{\rho_i g_{ti}(\mathbf{r});\mathbf{r}_1\}]-\mu^{HS}_{i,ex}(\{\rho_i\}))+\tilde{\gamma}_{ti}(r)$, requires the excess chemical potential functional $\mu^{HS}_{i,ex}$ and the auxiliary function $\tilde{\gamma}_{ti}(r)=\Sigma_j\rho_j\int d\mathbf{r}' c^{(2),HS}_{ij}(\{\rho_i\};|\mathbf{r}-\mathbf{r}'|)h_{tj}(\mathbf{r}')$, where $c^{(2),HS}_{ij}$ is the Percus Yevick HS direct correlation function and h_{tj} the test particle-j particle total correlation function. We refer the reader to Rosenfeld's paper [59] for the expression of $\mu^{HS}_{i,ex}$ and to [46] for implementation details in our present case (see, also, Ref. [61] for HS near a hard wall). Besides the fact that the numerical evaluation of the b_{ij} is more involved than when one uses parametrized forms, the main difference is that an extra cycle is required by the convergence of the bridge function (note that its expression involves both the reference system and the correlation functions h_{tj} for the actual interactions u_{ij}). This method has been successfully applied by Kahl *et al.* [62] to various mixtures but they did not consider highly asymmetric ones.

This method shares with some DFT calculations [40,45] the use of Rosenfeld's functional, but in a quite different manner. The formal connection of Eqs. (6) and (13) with the DFT approach is detailed in Ref. [7]. In a strict DFT calculation, one uses the equation for the profile that results from the minimization of a given grand potential functional [63], while in the IE route, this equation for the profile is recast, through the test particle consistency in the form of a closure of the OZE with an imposed bridge functional [59]. This may have quite different consequences when solvent-solvent attractions are involved. While the DFT calculation uses directly the HS functional in the equation for the profile [unless some additional prescription is made for the attractive part [63]], the only assumption made in the RHNC/FMF closure is that the HS bridge functional (not function: recall that this functional depends on the correlation functions for the actual interactions u_{ij}) is universal. Since these interactions appear directly in the closures of the OZE, Eq. (8), the RHNC/FMF can work even for a non-hard-sphere solvent. In some ''critical'' cases involving very fine details of the various correlations, it needs, however, to be improved [46]. On the whole, the treatment of solvent-solvent attractive forces involves thus a much weaker assumption than the pure neglect of the solvent-solvent attractive contributions to the free energy functional. In any case, improvements of the functional for treating the attractive contributions can readily be incorporated into the IE approach through the corresponding bridge functional.

Finally, we mention here that under conditions where the disturbance of the distribution of the solvent around an isolated solute, induced by an approaching second solute, is expected to be weak (low ρ^* and no long range solute-solvent interaction), Φ^{eff} can be computed more simply by

integrating the mean force $F^{eff}(R_{12})=\int d\mathbf{r}\nabla u_{12}(\mathbf{r}-\mathbf{R}_1)\rho^1(\mathbf{r};\mathbf{R}_1,\mathbf{R}_2)$ and replacing the actual solvent density about a pair of solutes at $(\mathbf{R}_1,\mathbf{R}_2)$ by

$$\rho^1(\mathbf{r};\mathbf{R}_1,\mathbf{R}_2)=\rho_1 g_{12}(|\mathbf{r}-\mathbf{R}_1|)g_{12}(|\mathbf{r}-\mathbf{R}_2|) \qquad (14)$$

(superposition approximation [64]) where $g_{12}(r)$ is the solvent-isolated solute pdf.

D. Models with attractions

Since the purpose of the present work is to discuss the microscopic parameters that exert the most influence on the phase behavior rather than to investigate a specific system (see, for example, the study by similar techniques of the effective interaction in reverse micelles [65], the behavior of passivated nanoparticles [66] or the molecular dynamics study of Shinto *et al.* [67] of colloidal particles in alcohol-water mixtures), we consider here, as in our previous works, two simple models of spherically symmetric interactions, namely the solvent-solvent Lennard-Jones (LJ) potential (with parameters ϵ and σ):

$$u_{LJ}(r)=4\epsilon\left[\left(\frac{\sigma}{r}\right)^{12}-\left(\frac{\sigma}{r}\right)^{6}\right] \qquad (15)$$

and the solute-solvent Yukawa potential (parameters ϵ_{12}, D_{12}, and z_{12}):

$$u_{12}(r)=\begin{cases}\infty, & r<D_{12}\\ -\epsilon_{12}\exp\{-z_{12}(r-D_{12})\}/r, & r\geqslant D_{12}.\end{cases} \qquad (16)$$

For convenience, the following reduced parameters will be used: the solute/solvent diameter ratio $R=D_2/D_1^{HS}$ and the solute-solvent hard core diameter $D_{12}=\frac{1}{2}(D_1^{HS}+D_2)$ are defined from the solvent effective hard sphere diameter (in units of the LJ parameter σ)D_1^{HS}. For the definition of the latter we took $u_{LJ}(D_1^{HS})\sim 1.5k_BT$. The reduced solvent density is $\rho^*\equiv\rho\sigma^3$. $\epsilon^*\equiv\epsilon/k_BT$ is the reduced strength of the LJ potential. $\epsilon_{12}^*\equiv\epsilon_{12}/(D_{12}k_BT)$ is the reduced strength of the solvent-solute Yukawa potential and z_{12} its inverse range (units of $1/\sigma$).

These models of u_{11} and u_{12} should be appropriate to investigate the general trends associated with of a non-hard-sphere solvent interacting with a solute with variable solvophilicity, as this occurs with sterically stabilized silica particles in organic solvent or in some reverse micellar systems. We finally mention that the direct interaction u_{22} between the solutes must be added to Φ^{eff} in order to study the thermodynamics of the effective fluid. For simplicity, u_{22} was taken here as a pure hard core interaction. As emphasized in Refs. [65,68] a less brutal modeling of this direct interaction might be necessary for investigating the actual total effective interaction in real colloids.

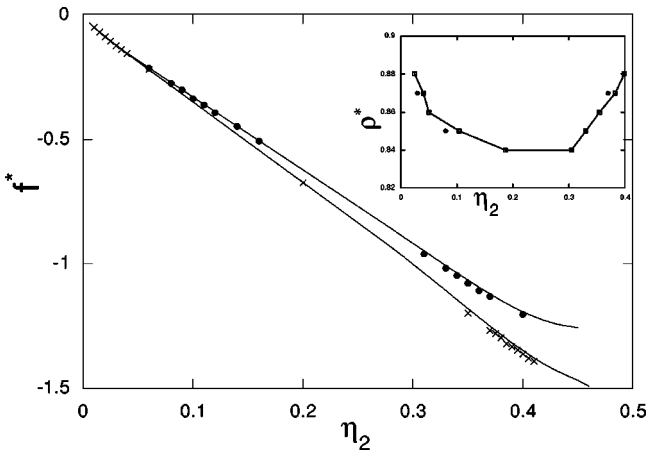

FIG. 1. Reduced free energy density $f^*\equiv\eta_2 F/N_2k_BT$ of the effective fluid versus solute packing fraction η_2. Size ratio, R=10; solvent effective HS diameter, $D_1^{HS}=0.94\sigma$; reduced LJ strength, $\epsilon^*=0.5$; reduced Yukawa strength, $\epsilon_{12}^*=8$; and inverse range, $z_{12}=2.5/\sigma$. Black circles, MC ($\rho^*=0.85$); crosses, MC ($\rho^*=0.87$). Lines: corresponding RHNC results. The inset shows the F-F coexistence data: black circles, MC; squares, RHNC [41] (the line is drawn to guide the eyes).

III. RESULTS AND DISCUSSION

A. Test of the RHNC free energy of the effective fluid

As noted in the Introduction, the first point that needs to be checked by simulation is the quality of the RHNC phase diagram. In the case of Φ^{eff} it is relatively long ranged and has an oscillatory behavior near contact. The fluid-fluid line is indeed very sensitive to the details of the interaction potential (the fluid-solid one somewhat less so). In the case of the depletion potential (pure hard spheres) the construction of the RHNC free energy with the $b_0(r)$ of Labik *et al.* [58] has already been compared [41] with the simulation data of Dijkstra *et al.* [3]. As with more standard potentials, good agreement was found for the depletion one (i.e., structured and short ranged). This method was, however, not tested in the case of interactions that combine both features. The simulations were done for $\rho^*=0.85$ and $\rho^*=0.87$ and used $\beta\Phi_{HNC}^{eff}$. At this stage, the particular closure used is irrelevant since the purpose is to check the phase diagram associated with a given Φ^{eff} of whatever origin. The parameters of the model (corresponding to one of those studied in Ref. [41]) are given in the figure caption and simulation details are given in the Appendix.

Figure 1 shows the free energies for both solvent densities. The agreement deteriorates somehow at high solute packing fractions η_2, but the RHNC remains accurate enough for computing the free energy for this kind of potential. As seen in the inset, the positions of the F-F line obtained by simulation and by the RHNC are practically the same. This test validates the RHNC route for computing the phase diagram for a given effective potential.

The second verification is relative to the quality of the RHNC/FMF effective potential resulting from a model of the actual interactions $u_{ij}(r)$. The good accuracy of the RHNC/FMF observed in our previous work [46] is confirmed here

TABLE I. Parameters of models *A* and *B*: $R=D_2/D_1^{HS}$, solute/solvent diameter ratio; $\epsilon^*\equiv\epsilon/k_BT$, reduced strength of the solvent-solvent LJ potential. D_1^{HS}: solvent effective hard sphere diameter in units of the LJ parameter σ. $\epsilon_{12}^*\equiv\epsilon_{12}/(D_{12}k_BT)$: reduced strength of the solvent-solute Yukawa potential. z_{12}: inverse range of the Yukawa potential in units of $1/\sigma$. The solute-solvent hard core diameter is $D_{12}=\frac{1}{2}(D_1^{HS}+D_2)$.

	R	ϵ^*	D_1^{HS}	ϵ_{12}^*	z_{12}
A	10	0.55	0.94	8	2.5
B	10	0.60	0.94	8	2.5

by new data for $R=10$ presented in the last section of this paper (although the present study is not concerned with this situation; see, however, the case of a solvophobic macroparticle for which the agreement with simulation was only qualitative [46]).

The two steps of the effective fluid approach are now validated. We can thus explore the changes induced by models of $u_{ij}(r)$ with attractive contributions.

B. Relative stability of the fluid-fluid and fluid-solid transitions

To illustrate specific behavior resulting from attractive contributions to the potentials $u_{ij}(r)$, we computed the phase diagram for two different models referred to as *A* and *B* (the associated parameters are given in Table I). These models differ by the strength of the solvent-solvent LJ interaction ($\epsilon^*=0.55$ for *A* and $\epsilon^*=0.60$ for *B*). For both models, the phase diagrams [Figs. 2(a) and 2(b)] were computed by using Φ_{RHNC}^{eff}. For model *B*, the result obtained with Φ_{HNC}^{eff} that is much simpler to compute is also shown. We simply note here that HNC is correct at the qualitative level but the coexistence lines are shifted at lower solvent packing fraction, a consequence of the overestimation of the attractive contribution in Φ_{HNC}^{eff}.

While the two models are quite similar, the resulting phase behavior is significantly different. For model *B*, the fluid-fluid (F-F) transition becomes stable with respect to the fluid-solid (F-S) one for $0.70\leqslant\rho^*\leqslant0.72$. For model *A*, the F-F coexistence line is always within the F-S one, that is the fluid-fluid transition is metastable. In fact, an increase of ϵ^* shifts both lines to lower ρ^* but the critical point for the F-F transition being more shifted, the relative stability of the two lines is inverted. This confirms the conjecture made in our previous work from Φ_{HNC}^{eff} [41]. To gain a better understanding of these features, we show in Figs. 3(a) and 3(b) the corresponding effective potentials Φ_{RHNC}^{eff} at selected values of ρ^*.

In both cases, Φ^{eff} exhibits a relatively long range attractive tail ($\sim0.5D_2$ after contact). This observation is important since the extent of the liquid domain is known to increase with the range of the attraction (see, for example, Refs. [60,69,70]). On the other hand, Φ^{eff} shows an attractive primary well at contact separated from the secondary well at $r\sim D_2+D_1^{HS}$ by a repulsive barrier, as with the HS depletion potential. Although the link between the interaction

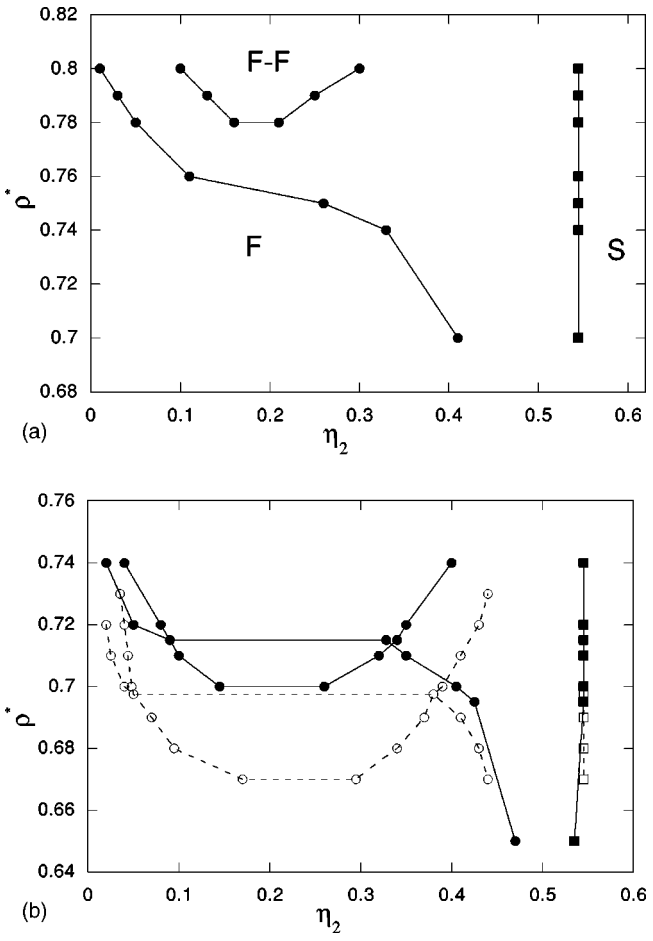

FIG. 2. (a) Phase diagram for Φ_{RHNC}^{eff} in the $(\rho^*-\eta_2)$ plane for model *A*. F-F denotes the metastable fluid-fluid domain. *F* denotes the stable fluid phase. *S* denotes the stable solid phase. Dots, RHNC; squares, VPT. ρ^* is the solvent density in the reservoir and η_2 the solute packing fraction. (b) Phase diagrams in the $(\rho^*-\eta_2)$ plane for model *B*. Symbols: same as (a). Solid lines, Φ_{RHNC}^{eff}; dashed lines, Φ_{HNC}^{eff}.

potential and the phase diagram is not trivial because of the competition between enthalpy and entropy, the overall aspect of the phase diagram may tentatively be explained by the competing effects of these two features of Φ^{eff}. When ρ^* increases, the short range structure of Φ^{eff} due to the solvent layering near the surface of the solutes becomes more pronounced (the attractive well at contact being deeper and the repulsive barrier higher). Since the ''depletion'' effects are, however, lower than with pure hard spheres with the same values of *R* and ρ^*, one expects the F-S transition to be delayed to higher ρ^* both for *A* and *B*. The different positions of the F-S lines for the two models can be attributed to the repulsive barrier for $r\leqslant D_2+D_1^{HS}$ that prevents the solutes from making contact. This is higher in case *A* ($\sim4.8k_BT$ for $\rho^*=0.8$) than in case *B* ($3k_BT$ for $\rho^*=0.74$), the global attraction being the same at these densities. As a result the F-S transition of model *A* is delayed to a higher solvent packing fraction than in case *B*. At the same time, one observes that the depth of the wells at long range increases more than the corresponding repulsive barriers. As

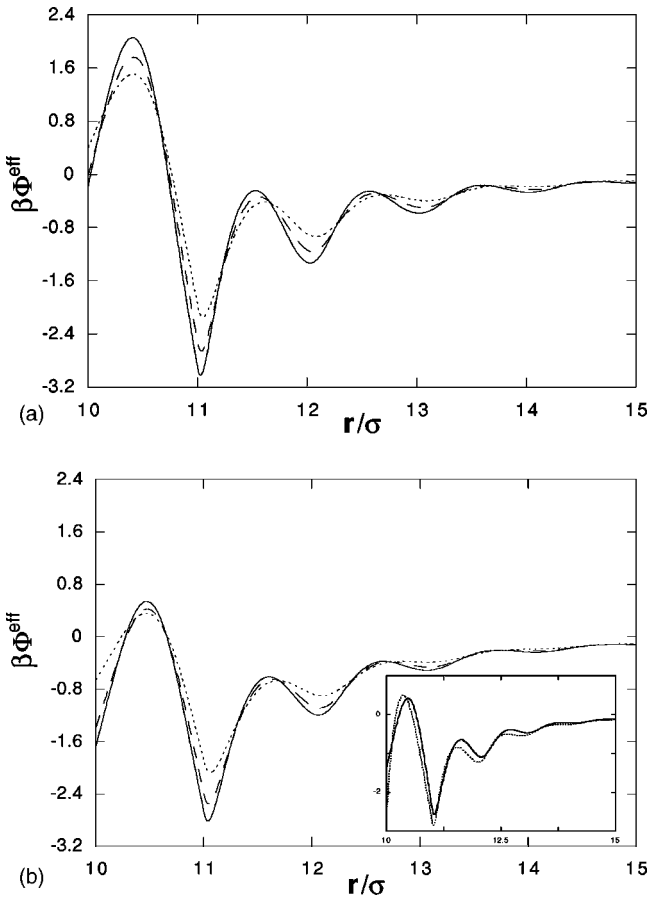

FIG. 3. (a) Reduced effective pair potential $\beta\Phi^{eff}_{RHNC}$ for model *A*. Dotted line, $\rho^*=0.7$; dashes, $\rho^*=0.76$; solid line, $\rho^*=0.8$. (b) Reduced effective pair potential $\beta\Phi^{eff}_{RHNC}$ for model *B*. Dotted line, $\rho^*=0.65$; dashes, $\rho^*=0.71$; solid line, $\rho^*=0.74$. Inset: comparison with HNC for $\rho^*=0.71$: solid line, Φ^{eff}_{RHNC}; dotted line, Φ^{eff}_{HNC}.

a result, Φ^{eff} becomes on the whole more attractive at long range in both models. However, higher values of ρ^* are needed in case *A* to obtain the same global attraction than in case *B* [see Figs. 3(a), 3(b)]. As a result, the F-F transition occurs also at higher ρ^* but the shift of the F-S and F-F lines is not the same for *A* and *B*. The reason is that Φ^{eff}_B cannot be deduced from Φ^{eff}_A by a mere increase of ρ^*. Indeed, the structure which is superimposed on the overall attractive tail and that is due to the layering of the solvent particles between the solutes is more readily smoothed by an increase of ϵ^* in case *B* (see the discussion of Fig. 8 in Ref. [34]). As a consequence, the widening of the region where Φ^{eff}_B is attractive is eventually strong enough to favor the liquid phase, as for ordinary (structureless) potentials. The comparison of the phase boundaries [Fig. 2(b)] obtained with Φ^{eff}_{RHNC} and Φ^{eff}_{HNC} gives weight to this scenario since the two main features of the effective interaction are magnified by the HNC closure [Fig. 3(b)].

Because of the importance of the long range behavior of the effective interaction, we discuss below in more detail the role of the solvent self-attraction.

C. Effect of solvent-solvent long range correlations

In the preceding section we have shown that the long range attractive tail of the effective potential is quite sensitive to the parameter ϵ^* of the solvent-solvent LJ potential. A change in ϵ^* affects both the depth of the well and the attraction range. Long range correlations between the solvent particles are suspected to favor their removal from the inner region between the solutes due to a stronger attraction by the bulk [34] (see also, for example, the discussion of Jamnik *et al.* [26] of the role of the solvent stickiness). Because of the ensuing smoothing of the oscillations in Φ^{eff}, it is useful to study more specifically the influence of the range of the solvent-solvent interaction. To this end, we consider here the truncated and shifted LJ potential, at a cutoff distance r_{cut}:

$$u_{11}(r)=\begin{cases} u_{LJ}(r)-u_{LJ}(r_{cut}), & r\leqslant r_{cut} \\ 0, & r>r_{cut}. \end{cases}$$

The strength of the LJ potential is now $\epsilon^*=0.7$ and for simplicity D_1^{HS} was taken equal to σ instead of 0.94σ in the preceding section. The corresponding size ratio is $R=10$, viz., $D_2=10\sigma$. The solvent packing fraction is $\rho^*=0.6$ and the Yukawa solute-solvent parameters were fixed at $\epsilon^*_{12}=9$ and $z_{12}=2.5/\sigma$. The corresponding Φ^{eff}_{RHNC} was computed for $r_{cut}=2.5\sigma$, 4σ, and 40.96σ. As seen in Fig. 4, the attractive tail of Φ^{eff} is rather sensitive to the range of $u_{11}(r)$. For $r_{cut}=2.5\sigma$ and $r_{cut}=4\sigma$ the effective force between two solute particles in the solvent bath was also determined by Monte Carlo simulation [Fig. 4(b)]. As in our previous work, we used the same method (details are given in the Appendix) as that used by Dickman *et al.* [71] for hard spheres. The good agreement observed for both values of r_{cut} [Fig. 4(a)] confirms that this spectacular effect is real and not an artifact of an approximate closure of the integral equations. For $r_{cut}=2.5\sigma$, the effective interaction is repulsive at long distances, whereas it becomes attractive when r_{cut} is increased to 4σ. This gives some support to the physical interpretation based on the attraction from the bulk of the interstitial solvent that was suggested above. It must be stressed here that having at our disposal an accurate theoretical method is an essential point for computing the phase diagram. Indeed, the length of simulations becomes really prohibitive when the range of the solvent-solvent interaction increases so they can be used only for validation purposes.

Since the effective potential is essentially determined by the solvent-solvent and solute-solvent correlations [see Eqs. (7)–(13) and the discussion of the magnitude of b_{22} in Ref. [46]], we compared $g_{11}(r)$ and $g_{12}(r)$ obtained by simulation and by IE. The good agreement between simulation and IE confirms the accuracy of the FMF bridge functions. While $g_{11}(r)$ is barely affected by the cutoff, the contact value of $g_{12}(r)$ is sensitive to r_{cut} (Fig. 5). It decreases when the range of the LJ potential increases, a result consistent with the extrapolation to finite size ratios of the contact value theorem [34,65]. As a result, weaker ''depletion'' effects may be expected because fewer interstitial solvent particles are involved, consistent with the observations made in the pre-

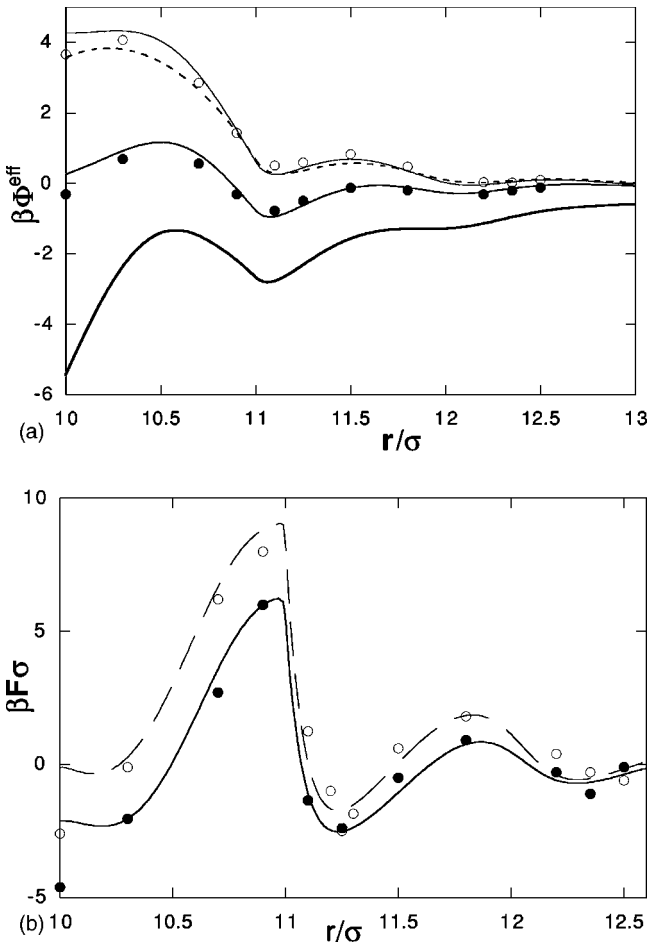

FIG. 4. (a) Reduced effective pair potential $\beta\Phi^{eff}$ for $R=10$ and $\rho^*=0.6$ and different cutoff distances of the solvent-solvent LJ potential. Solid lines from top to bottom: RHNC/FMF with $r_{cut}=2.5$, $r_{cut}=4$ and no cutoff. The dashed line shows the result obtained with g_{12}^{RHNC} (see Fig. 5) in Eq. (14) for $r_{cut}=4$. MC result from the integration of the effective force [Fig. 4(b)] (with extension by $\beta\Phi_{RHNC}^{eff}$ beyond 12.5σ): empty circles, $r_{cut}=2.5$; filled circles, $r_{cut}=4$. (b) Reduced effective force for $R=10$ and $\rho^*=0.6$ and different values of r_{cut}. Empty circles (MC) and dashed line (Φ_{RHNC}^{eff}), $r_{cut}=2.5$; filled circles (MC) and solid line (Φ_{RHNC}^{eff}), $r_{cut}=4$.

ceding section. The subtle long range behavior of Φ^{eff} is, however, more difficult to guess from these tiny structural changes [46]. This is confirmed by a comparison with the Φ^{eff} computed from the superposition approximation [see Eq. (14)] which involves only the solvent distribution g_{12} about an isolated solute. Figure 4 shows that this method fails to predict good trends at long distance, $\Phi_{\mathrm{sup}}^{eff}$ being insensitive to changes of r_{cut}. This shows that Φ^{eff} is determined by the fine structure of g_{11} and g_{12} which are coupled by the OZE. This coupling with the bulk fluid seems to be amplified when the range of the solvent-solvent interaction is the biggest [65]. Arguments of a similar nature have been invoked in Ref. [45] to analyze some combinations of solvent-solvent and solute-solvent attractions.

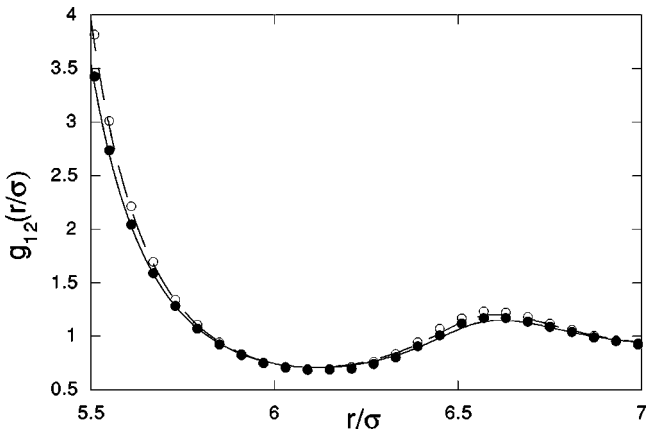

FIG. 5. Solvent-solute pair distribution function $g_{12}(r/\sigma)$ for $R=10$ and $\rho^*=0.6$ vs reduced distance r/σ. Same caption as Fig. 4(b).

IV. CONCLUSION

This study has shown that the complexity of the phase behavior of real colloidal mixtures can be restored by taking into account the specificity via models of the interactions between components incorporating some aspects of real interactions, namely, a short range repulsion and an attractive tail. The most immediate consequence of this refined modeling is that the F-F phase can be stable even at high packing fraction of solvent particles. This can be explained by a competition between entropic and enthalpic contributions to the effective potential which produces two features of the effective potential.The first one is related to the steric effects as in pure hard sphere systems. The second and more specific one results from the competition between the solute-solvent attraction which tends to favor the solvation of the solutes and the self-attraction of the solvent which makes the effective interaction between solutes more attractive at long range. By comparison with simulation, it was also confirmed that significant changes of the effective potential might result from seemingly benign alteration of the parameters of the interactions. Besides making questionable the relevance of the hard sphere model to the study of many real colloidal suspensions, especially when it concerns the solvent-solvent and solute-solvent interactions, this state of affairs shows that further investigations are clearly required. This observed sensitivity emphasizes first the care that should be taken in the interpretation of some experimental observations. It also calls for the development of more accurate theoretical methods. On the other hand, a refined description of the interactions might be required in order to consider—for example—actually nonspherical solvent particles. Finally, theoretical progress in these directions would eventually enable devising practical methods for controlling the stability of the various phases.

ACKNOWLEDGMENT

The simulations were partly supported by a grant of CPU time by the CINES (Montpellier, France).

APPENDIX: SIMULATION DETAILS

1. Computing the free energy

Since the free energy cannot be obtained directly in an (NVT) Monte Carlo simulation, we employed the same method as in Ref. [3]. It uses thermodynamic integration via a charging parameter λ defined by

$$\phi_\lambda = \phi^0 + \lambda \phi^{eff}$$

$\lambda = 0$ corresponds to the HS reference potential and $\lambda = 1$ to the full effective potential. The free energy of the effective fluid reads thus

$$F = F_0 + \int_0^1 \left\langle \sum_{i<j} \Phi^{eff}(r_{ij}) \right\rangle_{(N_2,V,\Phi_\lambda)} d\lambda. \qquad \text{(A1)}$$

For the free energy F_0 of the HS system, we took the Carnahan-Starling expression [71]. $\langle \Sigma_{i<j} \Phi^{eff}(r_{ij}) \rangle_{(N_2,V,\Phi_\lambda)}$ is the canonical average of $\Sigma_{i<j} \Phi^{eff}(r_{ij})$ for N_2 solutes interacting with Φ_λ (this method is also useful to extrapolate the RHNC free energy in the nonconvergence domain).

We estimated that seven values of λ per solute packing fraction η_2 were sufficient to perform the numerical integration. Because of the relatively long range of the effective interaction, we used 256 particules for $\eta_2 > 0.2$ and 108 particles for $\eta_2 < 0.2$. To reduce the simulation time, a parallelized algorithm with seven simultaneous simulations was used to obtain the free energy for a given η_2. About 15 values of η_2 were next used to draw the common tangent [that is, 105 (NVT) simulations per value of ρ^*].

2. Computing the effective potential

Φ^{eff} was obtained by integrating the force between two solute particles at a distance D in a bath of solvent as proposed by Dickman *et al.* [72]. The effective force is given by

$$F_z(D) = \int \vec{\nabla} u_{12}(|\vec{r} - \vec{R}_1|) \vec{k} dN_1, \qquad \text{(A2)}$$

where $\vec{k}$ is a unit vector along the line connecting the centers of the solute particles. For solute-solvent interaction with a hard core and an attractive tail, the force reads

$$F_z(D) = \left\langle \sum_i^{N_1} \cos\theta \right\rangle_{contact} + \left\langle \sum_i^{N_1} \frac{\partial u_{12}(u)}{\partial u} \cos\theta \right\rangle, \qquad \text{(A3)}$$

where θ is the angle $(\vec{k}, \vec{r} - \vec{R}_1)$. The first term in Eq. (A3) relative to the HS contribution is computed as the thermal average of the sum of $\cos\theta$ over the solvent particles in sufficiently small shells near contact (here the thickness of the shell is 0.02σ). The actual contact value is obtained by extrapolation as in Ref. [72]. The effective force was determined up to $D = 12.5\sigma$, a separation at which the oscillations are damped enough and about ten points (NVT simulations) were used to integrate the force (beyond $12.5\sigma \Phi^{eff}_{RHNC}$ was used). Due to the range of the solvent-solvent interaction and that of the resulting effective force, very large boxes were considered. For the two models the box size was $32 \times 18 \times 18\sigma^3$ and the number of small particles corresponding to $\rho^* = 0.6$ was $N_1 = 5633$. The value of ρ^* was checked by measuring the average density at the edges of the box. For comparison, Dickman *et al.* used a box size $22 \times 16 \times 16\sigma^3$ for hard spheres with same ρ^* [72]. A standard neighbor list was employed [73]. Finally for a given separation between the solutes, the calculation of the force for $r_{cut} = 4$ took three days for 200 000 production cycles and an equivalent phase of equilibration on our workstations. Note that the efficiency of the algorithm, namely, that relative to the neighbor list, decreases dramatically when the solvent-solvent interaction range increases [73]. This renders impractical simulations beyond $r_{cut} = 4$.

The solvent-solute pdf g_{12} was obtained by using a standard (NVT) simulation of the solvent in the field of the big Yukawa particle fixed at the center of a cubic box with size $(18\sigma)^3$.

[1] R. J. Hunter, *Foundations of Colloid Science* (Oxford University Press, New York, 1987).

[2] W. B. Russel, D. A. Saville, and W. R. Showalter, *Colloidal Dispersion* (Cambridge University Press, Cambridge, UK, 1989).

[3] M. Dijkstra, R. van Roij, and R. Evans, Phys. Rev. Lett. **81**, 2268 (1998); **82**, 117 (1999); Phys. Rev. E **59**, 5744 (1999).

[4] N. G. Almarza and E. Enciso, Phys. Rev. E **59**, 4426 (1999).

[5] C. Caccamo, Phys. Rep. **274**, 1 (1996).

[6] B. Gotzelmann, R. Evans, and S. Dietrich, Phys. Rev. E **57**, 6785 (1998).

[7] R. Roth, R. Evans, and S. Dietrich, Phys. Rev. E **62**, 5360 (2000).

[8] J. I. Siepmann and D. Frenkel, Mol. Phys. **75**, 59 (1992); D. Frenkel, G. C. A. M. Mooij, and B. Smit, J. Phys.: Condens. Matter **3**, 3053 (1991).

[9] C. Dress and W. Krauth, J. Phys. A **28**, L597 (1995); A. Buhot and W. Krauth, Phys. Rev. Lett. **80**, 3787 (1998).

[10] L. Lue and L. V. Woodcock, Mol. Phys. **96**, 1435 (1999).

[11] G. Jackson, J. S. Rowlinson, and F. J. van Swol, J. Phys. Chem. **91**, 4907 (1987).

[12] F. J. Rogers and D. A. Young, Phys. Rev. A **30**, 999 (1984).

[13] P. Ballone, G. Pastore, G. Galli, and D. Gazzillo, Mol. Phys. **59**, 275 (1986).

[14] P. Attard and G. N. Patey, J. Chem. Phys. **92**, 4970 (1990).

[15] Y. Rosenfeld, Phys. Rev. Lett. **72**, 3831 (1994).

[16] T. Biben and J. P. Hansen, Phys. Rev. Lett. **66**, 2215 (1991).

[17] S. Asakura and F. Oosawa, J. Chem. Phys. **22**, 1255 (1954).

[18] A. Vrij, Pure Appl. Chem. **48**, 471 (1976).

[19] J. L. Lebowitz and J. S. Rowlinson, J. Chem. Phys. **41**, 133 (1964).

[20] J. K. Percus and G. J. Yevick, Phys. Rev. **110**, 1 (1958).

[21] S. H. Chen, J. Rouch, F. Sciortino, and P. Tartaglia, J. Phys.: Condens. Matter **6**, 10855 (1994).
[22] C. G. de Kruif, P. W. Rouw, W. J. Briels, M. H. G. Duits, A. Vrij, and R. P. May, Langmuir **5**, 422 (1989).
[23] B. Lemaire, P. Bothorel, and D. Roux, J. Phys. Chem. **87**, 1023 (1983); S. Brunetti, D. Roux, A. M. Bellocq, G. Fourche, and P. Bothorel, *ibid.* **87**, 1028 (1983).
[24] R. J. Baxter, J. Chem. Phys. **48**, 2770 (1968).
[25] C. Robertus, W. H. Philipse, J. G. H. Joosten, and Y. K. Levine, J. Chem. Phys. **90**, 4482 (1989).
[26] A. Jamnik, D. Bratko, and D. Henderson, J. Chem. Phys. **94**, 8210 (1991).
[27] M. H. G. M. Penders and A. Vrij, Physica A **173**, 532 (1991); M. H. G. M. Penders and A. Vrij, Prog. Colloid Polym. Sci. **88**, 1 (1992).
[28] C. Regnaut, S. Amokrane, and Y. Heno, J. Chem. Phys. **102**, 6230 (1995); S. Amokrane and C. Regnaut, *ibid.* **106**, 376 (1997).
[29] E. Dickinson, J. Chem. Soc. Faraday Trans. **91**, 4413 (1995).
[30] A. Jamnik, J. Chem. Phys. **105**, 10511 (1996).
[31] P. Attard, D. Wei, G. N. Patey, and G. M. Torrie, J. Chem. Phys. **93**, 7360 (1990).
[32] D. Henderson and M. Plishke, J. Chem. Phys. **97**, 7822 (1992).
[33] M. Kinoshita, S. Iba, and M. Harada, J. Chem. Phys. **105**, 2497 (1996); M. Kinoshita, Mol. Phys. **94**, 485 (1998).
[34] S. Amokrane, J. Chem. Phys. **108**, 7459 (1998).
[35] R. Garibay-Alonso, J. M. Mendez Alcaraz, and R. Klein, Physica A **235**, 159 (1997).
[36] H. H. von Grünberg and R. Klein, J. Chem. Phys. **110**, 5421 (1999).
[37] E. Allahyarov, I. D'Amico, and H. Löwen, Phys. Rev. Lett. **81**, 1334 (1998).
[38] A. A. Louis, R. Finken, and J. P. Hansen, Phys. Rev. E **61**, 1028 (2000).
[39] A. A. Louis and R. Roth, J. Phys.: Condens. Matter **13**, L777 (2001).
[40] R. Roth, R. Evans, and A. A. Louis, Phys. Rev. E **64**, 051202 (2001).
[41] J. Clement-Cottuz, S. Amokrane, and C. Regnaut, Phys. Rev. E **61**, 1692 (2000).
[42] T. Biben and J. P. Hansen, Physica A **235**, 142 (1997).
[43] J. G. Malherbe and S. Amokrane, Mol. Phys. **97**, 677 (1999).
[44] H. Shinto, M. Miyahara, and K. Higashitani, J. Colloid Interface Sci. **209**, 79 (1999).
[45] A. A. Louis, E. Allahyarov, H. Löwen, and R. Roth, Phys. Rev. E **65**, 061407 (2002).
[46] S. Amokrane and J. G. Malherbe, J. Phys.: Condens. Matter **13**, 7199 (2001); **14**, 3845(E) (2002).
[47] T. L. Hill, *Statistical Mechanics* (Dover Publications, New York, 1997).
[48] F. Lado, S. M. Foiles, and N. W. Aschroft, Phys. Rev. A **28**, 2374 (1983).
[49] Ph. Germain and S. Amokrane, Phys. Rev. E **65**, 031109 (2002).
[50] J. P. Hansen and I. R. MacDonald, *Theory of Simple Liquids* (Academic Press, London, 1976).
[51] T. Biben, P. Bladon, and D. Frenkel, J. Phys.: Condens. Matter **8**, 10 799 (1996).
[52] P. Attard, J. Chem. Phys. **95**, 4471 (1991).
[53] J. G. Malherbe and S. Amokrane, Mol. Phys. **99**, 355 (2001).
[54] F. Lado, Phys. Lett. **89**, 196 (1982).
[55] E. Lomba, Mol. Phys. **68**, 87 (1989); E. Lomba and N. G. Almarza, J. Chem. Phys. **100**, 8367 (1994).
[56] Y. Rosenfeld, Mol. Phys. **94**, 929 (1998).
[57] A. Malijevski and S. Labik, Mol. Phys. **60**, 663 (1987); S. Labik and A. Malijevski, *ibid.* **67**, 431 (1989).
[58] S. Labik, A. Malijevski, and P. Vonka, Mol. Phys. **56**, 709 (1985).
[59] Y. Rosenfeld, J. Chem. Phys. **98**, 8126 (1993).
[60] M. Hasegawa, J. Chem. Phys. **108**, 208 (1998).
[61] R. Roth and S. Dietrich, Phys. Rev. E **62**, 6926 (2000).
[62] G. Kahl, B. Bildstein, and Y. Rosenfeld, Phys. Rev. E **54**, 5391 (1996).
[63] R. Evans, in *Fundamentals of Inhomogeneous Fluids*, edited by D. Henderson (Marcel Dekker, New York, 1992), p. 23; Adv. Phys. **28**, 143 (1979).
[64] J. G. Kirkwood, J. Chem. Phys. **3**, 300 (1935).
[65] M. Bouaskarne, S. Amokrane, and C. Regnaut, J. Chem. Phys. **114**, 2442 (2001).
[66] S. A. Egorov and E. Rabani, J. Chem. Phys. **115**, 617 (2001).
[67] H. Shinto, M. Miyahara, and K. Higashitani, Langmuir **16**, 3361 (2000).
[68] S. Amokrane and M. Bouaskarne, J. Chem. Phys. **112**, 11107 (2000).
[69] M. H. Hagen and D. Frenkel, J. Chem. Phys. **101**, 4096 (1994).
[70] C. Rascon, G. Navascues, and L. Mederos, Phys. Rev. B **51**, 14899 (1995).
[71] N. F. Carnahan and K. E. Starling, J. Chem. Phys. **86**, 5683 (1969).
[72] R. Dickman, P. Attard, and V. Simonian, J. Chem. Phys. **107**, 205 (1997).
[73] M. P. Allen and D. J. Tildesley, *Computer Simulation of Liquids* (Oxford Science Publication, Oxford, 1987).